Biomedical Signal Processing and Control 8 (2013) 23–29

Contents lists available at SciVerse ScienceDirect

Biomedical Signal Processing and Control

journal homepage: www.elsevier.com/locate/bspc

Fractal analysis of knee-joint vibroarthrographic signals via power spectral analysis☆

Rangaraj M. Rangayyan[a,*], Faraz Oloumi[a], Yunfeng Wu[b], Suxian Cai[b]

[a] Department of Electrical and Computer Engineering, Schulich School of Engineering, University of Calgary, Calgary, AB, Canada T2N 1N4
[b] Department of Communication Engineering, School of Information Science and Technology, Xiamen University, Xiamen, Fujian 361005, China

ARTICLE INFO

Article history:
Received 19 August 2011
Received in revised form 21 March 2012
Accepted 16 May 2012
Available online 6 June 2012

Keywords:
Articular cartilage deterioration
Fractal analysis
Fractal dimension
Knee joint sounds
Power spectrum analysis
Vibroarthrography

ABSTRACT

Parameters useful for the diagnosis of pathological processes leading to the deterioration of the articular cartilage surfaces of knee joints, such as osteoarthritis, may be derived from vibroarthrographic (VAG) signals. In the present work, we explore fractal analysis to parameterize the temporal and spectral variability of normal and abnormal VAG signals. The power spectrum analysis method was used with the $1/f$ model to derive estimates of the fractal dimension (FD). Classification accuracy of up to 0.74 was obtained with a single FD parameter, in terms of the area under the receiver operating characteristic curve (A_z), with a database of 89 VAG signals. Combinations of the features derived in the present work with other features we have reported upon recently, when used with several neural networks with radial basis functions, resulted in A_z values in the range [0.92, 0.96], with an exceptional case of perfect classification with $A_z = 1.0$. The proposed methods could help in the detection and monitoring of knee-joint pathology.

1. Introduction

1.1. Fractals and the 1/f model

One of the several definitions of fractals is based on geometric structures that have self-similarity at different scales of length [1–3]. Fractals lack any single scale of length, and have a noninteger (fractional) dimension, referred to as the fractal dimension (FD). Fractal geometry has been used to represent and synthesize several natural forms such as leaves, trees, mountains, clouds, and lunar craters. Fractal models are created iteratively, which makes them suitable for computer algorithms to simulate natural scenery. Wiener's geometric model of physical Brownian motion has been used as the basis for several algorithms to generate fractal images. In this model, the unpredictable variation of a quantity, V, over time, t, is viewed as a noise process, $V(t)$. The power spectral density (PSD), $P_V(f)$, is used to estimate the power of fluctuations at a given frequency, f, and also of the variations over a time scale of the order of $1/f$.

Any varying quantity, $V(t)$, with the best fitting line to its PSD, $P_V(f)$, varying as $1/f^{\beta}$ on a log–log scale, is referred to as $1/f$ noise; this is known as the inverse power law or the $1/f$ model. According to Voss [3], most natural phenomena under this model have β in the range of [0.5, 1.5]. The PSD of a noise process represented by Brownian motion or random walk varies as $1/f^2$; the power decreases quadratically with frequency. The trace of such a signal is a fractal curve. A direct relationship exists between the FD of the signal and the slope, β, of the best fitting line to its PSD on a log–log scale [3].

The fractional Brownian motion (fBm) model of Mandelbrot [1] has formed the basis of several mathematical models for computer generation of natural fractal scenery. Models based on fBm have been extended to two dimensions for the synthesis of Brownian surfaces and three dimensions to generate Brownian clouds [2].

Fig. 1 shows examples of signals, $V_H(t)$, generated as functions of an arbitrary time variable, t, based on the fBm model. The scaling of the traces is characterized by the scaling parameter H, known as the Hurst coefficient, in the range $0 \leq H \leq 1$. A high value of H close to 1 results in a relatively smooth signal. A low value of H produces a rougher trace. The variable H relates the changes in V, $\Delta V = V(t_2) - V(t_1)$, to differences in the time variable, $\Delta t = t_2 - t_1$, by the scaling law [3]

$$\Delta V \propto (\Delta t)^H. \quad (1)$$

Self-similar patterns repeat themselves under magnification. However, fBm traces repeat statistically only when t and V are magnified by different amounts. If t is magnified by a factor r as rt, the

☆ A preliminary version of this paper was presented at the 10th IEEE International Conference on Information Technology and Applications in Biomedicine (ITAB 2010), Corfu, Greece, November 2010.

* Corresponding author. Tel.: +1 403 220 6745; fax: +1 403 282 6855
E-mail address: ranga@ucalgary.ca (R.M. Rangayyan).

1746-8094/$ – see front matter © 2012 Elsevier Ltd. All rights reserved.
http://dx.doi.org/10.1016/j.bspc.2012.05.004

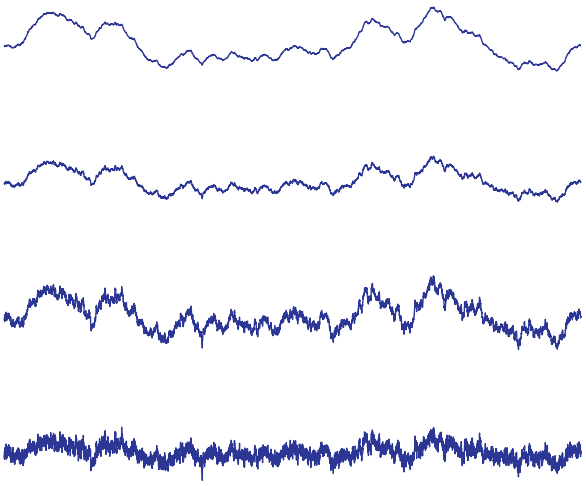

Fig. 1. Examples of signals generated based on the fBm model for different values of H and FD. Top to bottom: $H = 0.9, 0.6, 0.4, 0.1$; model FD = 1.1, 1.4, 1.6, 1.9; estimated FD = 1.104, 1.404, 1.604, 1.903.

value of V is magnified by the factor r^H and becomes $r^H V$. Nonuniform scaling of this nature is known as self-affinity [1]. The zero-set of an fBm signal is the intersection of the signal with the horizontal axis. The zero-set is a set of disconnected points with a topological dimension of zero and fractal dimension, D_0, given by [3]

$$D_0 = 1 - H. \tag{2}$$

The zero-set of a self-affine signal is self-similar; different estimates of D_0 will yield the same result. The FD of the signal is related to D_0 as

$$\mathrm{FD} = D_0 + 1, \tag{3}$$

and to the scaling parameter, H, as

$$\mathrm{FD} = 2 - H. \tag{4}$$

1.2. Fractal behavior of physiological signals

Fractal properties have been observed in several physiological structures and processes. Several anatomical structures have fractal-like appearance: the coronary arteries, venous branching patterns, bronchial trees, certain muscle-fiber bundles, and the His-Purkinje network in the ventricles [4]. The branching pattern of the His-Purkinje network of conduction pathways provides an efficient way to distribute the depolarization stimulus to the ventricles. The electrogenesis of the QRS complex in the electrocardiogram (ECG) has been modeled by using a fractal-like conduction system. The normal QRS complex has been shown to follow an inverse-power-law distribution of frequency content in the log–log scale [5]; this property has been noted as being consistent with depolarization of the myocardium by a self-similar branching network [4]. Studies of such branching networks used to depolarize a network of cells via computer modeling have shown that, after 10 generations of branching, it is possible to simulate realistic QRS complexes [6]. The frequency content of QRS complexes has been shown to be affected by changes in the geometry of the branching network.

Goldberger et al. [5,7] showed that the rhythm of a healthy heart beat is not highly regular, but is, instead, a temporal fractal with a high degree of variability in the heart rate. The PSD of a time-series representation of the heart rate follows the inverse power law. It has been shown that, in the case of time series of heart rate, the loss of physiological complexity can lead to greater regularity. The phenomena associated with fractals, self-similar scaling, $1/f$ noise, and inverse-power-law distributions offer interesting models as well as useful methods to characterize physiological processes and biomedical signals [7].

Li et al. [8] applied a method of fractal and wavelet-based spectral analysis to analyze electroencephalographic (EEG) signals of rats. It was hypothesized that variations in FD-related parameters, such as the Hurst and spectral exponents, can be used to describe the dynamic characteristics of the brain in different states, in particular before seizures. They found that the method revealed characteristic signs of an approaching seizure, including the emergence of long-range correlation and decrease in the FD value. Liang et al. [9] applied the Hurst exponent, extracted from EEG recordings, as a measure of the effects of anesthesia on brain activity. The maximal overlap discrete wavelet transform was used to suppress the effects of artifacts in the EEG and the scaling properties of the data in designated frequency bands were calculated prior to estimation of the Hurst exponent. It was observed that the Hurst exponent (especially in low-frequency bands) decreased when anesthesia deepened and that it is a useful measure for estimating the depth of anesthesia.

Shah et al. [10] studied acceleration signals obtained from finger joints of patients with calcium pyrophosphate deposition disease, rheumatoid arthritis, or spondyloarthropathy of the finger joint. The ruler method was used to estimate FD. The results showed that there were significant differences between the FD values of acceleration signals from patients in the three categories. Specifically, the FD values of acceleration signals from the patients with calcium pyrophosphate deposition disease (1.709 ± 0.097) were higher than those of patients with rheumatoid arthritis (1.6 ± 0.069) or spondyloarthropathy (1.569 ± 0.081).

As indicated by the brief review given above, there is increasing interest in nonlinear dynamical analysis of biomedical signals using several recently developed methods related to fractals, chaos, and nonlinear modeling. See Stam [11] for a detailed review of nonlinear dynamical analysis of EEG and other signals. The recently developed methods of nonlinear dynamical analysis are expected to make it possible to study self-organization, pattern formation, and attractors of trajectories in the state space of nonlinear and complex systems that may not be captured by traditional linear methods.

1.3. Vibroarthrography of the knee joint

Several abnormal conditions that affect the knee joint are expected to cause variations in the vibroarthrographic (VAG) signal, which represents the sound or vibration emitted from the joint during flexion and/or extension [12–23]. Digital signal processing and pattern classification techniques have been used to analyze VAG signals and derive features that could be related to the roughness, softening, breakdown, or the state of lubrication of the articular cartilage surfaces. Such methods are expected to assist in noninvasive detection and diagnosis of knee-joint pathology [21–23]. Screening for knee-joint pathology using VAG signals could reduce the need for diagnostic arthroscopy. Such methods could also find use in monitoring the functional integrity or deterioration in natural as well as artificial (prosthetic) joints [18]. Detailed reviews of the literature on VAG signals and related topics are provided in two of our recent publications [21,24].

Imaging techniques such as computed tomography and magnetic resonance imaging have limited application in the diagnosis of knee-joint pathology, especially in repeated investigation or continued monitoring. Orthopedic specialists and surgeons are interested in methods for noninvasive screening of patients prior to the recommendation of procedures such as arthroscopy. To address this need, we are developing screening methods and systems for use in the clinic of a physician or an orthopedic specialist [21–23]. For this purpose, in the present paper, we explore the applicability

of fractal analysis via power spectral analysis (PSA) with the $1/f$ model [3] to classify VAG signals as normal or abnormal, that is, to perform screening [25]. Fractal analysis can assist in identifying nonspecific complexity of patterns in signals with a different approach as compared to well-known signal processing methods that have been applied to VAG and other biomedical signals in the past. Representing the nature of a power spectrum with only one feature or measure is an attractive proposition that leads to substantial reduction in the dimensionality of the feature space.

2. Materials

2.1. Synthesized fractal signals

To evaluate the performance of the PSA method, it is desirable to have a set of fBm signals with known FD. Two types of methods are available to generate fBm signals: approximation by spatial methods and approximation by spectral synthesis. The most reliable method is spectral synthesis by means of inverse Fourier filtering [26]. If a_k is the kth complex coefficient of the discrete Fourier transform (DFT), to obtain $P(f) \propto 1/f^{\beta}$, the condition is

$$E[|a_k|^2] \propto \frac{1}{k^{\beta}}, \tag{5}$$

where k denotes the frequency index corresponding to f. By randomly selecting coefficients that satisfy the stated condition and then taking their inverse DFT, we can obtain the corresponding signal in the time domain. In the present work, a direct implementation of the algorithm given by Saupe [26] was used to generate 110 synthetic signals, 10 for each value of H, with $0 \leq H \leq 1$ in intervals of 0.1. Fig. 1 shows four examples of the synthesized signals for $H = 0.9$, 0.6, 0.4, and 0.1; the corresponding model FD values are = 1.1, 1.4, 1.6, and 1.9. It is evident from the illustration that the variability and complexity of the signals increase as H decreases (or as FD increases).

2.2. Acquisition of knee-joint VAG signals

The database used in the present study consists of 89 signals, with 51 from normal volunteers (22 male, 29 female, age 28 ± 9.5 years) and 38 from subjects with knee-joint pathology (20 male, 28 female, age 35 ± 13.8 years). The normals were established by clinical examination and history. The abnormal signals were collected from symptomatic patients scheduled to undergo arthroscopy independent of the VAG studies. Informed consent was obtained from each subject. The experimental protocol was approved by the Conjoint Health Research Ethics Board of the University of Calgary.

Each subject sat on a rigid table in a relaxed position with the leg being tested freely suspended in air. The VAG signal was recorded by an accelerometer (model 3115a, Dytran, Chatsworth, CA), placed at the mid-patella position of the knee, as the subject swung the leg over an approximate angle range of 135° (approximately full flexion) to 0° (full extension) and back to 135° in 4 s [16]. The first half (approximately) of each VAG signal corresponds to extension and the second half to flexion of the leg.

The VAG signals were prefiltered (10 Hz to 1 kHz) and digitized at the sampling rate of 2 kHz. For the present study, each signal was normalized to the amplitude range [0, 1] and resampled to the length of 8192 samples by linear interpolation.

The abnormal cases in the database include chondromalacia of different grades at the patella, meniscal tear, tibial chondromalacia, and anterior cruciate ligament injuries, as confirmed during arthroscopic examination. The dataset available is not adequate to permit classification of the signals into various types or stages of pathology. The present study is aimed at screening only, that is, classification of the signals and the corresponding knee joints as normal or abnormal.

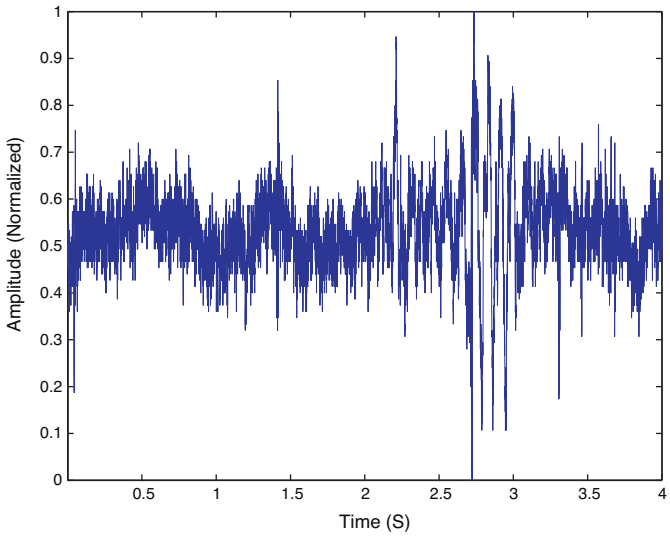

Fig. 2. Example of a normal VAG signal.

The present study uses the same dataset as that used in a few recent studies [20–23]. Figs. 2 and 3 show examples of normal and abnormal VAG signals.

3. Methods

3.1. FD via power spectral analysis

The best method available to estimate the FD of a self-affine signal is PSA. As explained in Section 1.1, an fBm signal has a PSD that follows the $1/f^{\beta}$ model. A high value of β indicates a rapid decrease in the high-frequency content of the signal. A self-affine fBm function in an E-dimensional Euclidean space has its PSD $P_V(f) \propto 1/f^{\beta}$, with [3]

$$\mathrm{FD} = E + 1 - H, \tag{6}$$

where

$$H = \frac{\beta - 1}{2}. \tag{7}$$

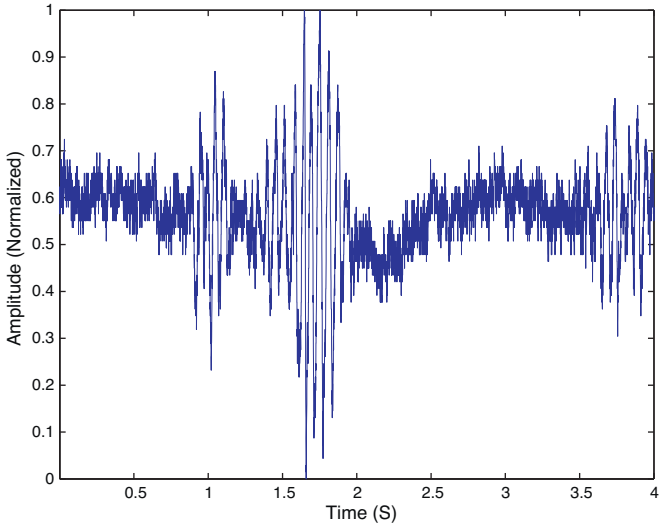

Fig. 3. Example of an abnormal VAG signal.

The FD, in terms of the spectral component, β, for a 1D signal with $E = 1$, is

$$\mathrm{FD} = \frac{5 - \beta}{2}. \quad (8)$$

In the present work, to estimate β, a Hanning window was first applied to the given VAG signal; then, the DFT of the windowed signal was calculated, and the squared magnitude of the result was used to obtain the PSD of the signal. The slope of the best fitting line to the log–log plot of PSD was then determined.

When applying the PSA method, it is important to specify an appropriate frequency range to obtain the linear fit. Low-frequency details related to any slow drift present in the signal as well as high-frequency content dominated by noise or artifacts in the signal should be disregarded in order to obtain accurate estimates of β and FD. When applying the PSA method to the fBm synthesized signals, PSD components spanning 1% of the total frequency range were removed at both the low and high ends of the positive frequency axis. For VAG signals, the frequency range to obtain the linear fit was varied between [10, 300] Hz and [10, 380] Hz to study the effect of the frequency range used on classification accuracy. This was based upon experimentation and analysis of the band of frequencies over which appreciable differences were observed between normal and abnormal VAG signals. (The VAG signals had been prefiltered to the range 10 Hz to 1 kHz at the time of data acquisition. Therefore, there is no useful information below 10 Hz.)

3.2. Analysis of segments of VAG signals

It is known that the VAG signal is nonstationary, and that it is appropriate to analyze segments of fixed or adaptive duration [14,16,21–23], or apply nonstationary signal processing techniques such as wavelets [20] and time-frequency distributions [17]. However, such methods increase the computational load. Furthermore, it is difficult, in practice, to associate parts of the knee joint affected by pathology to segments of VAG signals. The use of VAG signal segments of limited duration may lead to inaccuracies in the estimation of the PSD in low-frequency ranges. On the other hand, it has been observed that parts of VAG signals during certain portions of the swing cycle, especially extension, can provide features with higher discriminant capability than other parts [14,21–23]. To facilitate separate analysis of parts of VAG signals during extension and flexion and to derive multiple features, the PSA method was applied not only to get a parameter for the full VAG signal in each case (FD), but also to the first and second halves of the normalized duration (FD1h and FD2h, corresponding to extension and flexion), as well as to four segments with each spanning one quarter of the total duration (FD1q, FD2q, FD3q, and FD4q).

3.3. Feature analysis, selection, and pattern classification

The capability of each feature to discriminate between benign masses and malignant tumors was assessed by analyzing the area (A_z) under the receiver operating characteristic (ROC) curve [27,28] obtained using ROCKIT [29]. Features were also analyzed based on their p-values via the t-test [30]. Feature selection [31–33] was performed using the sequential forward selection (SFS) and sequential backward selection (SBS) methods incorporating logistic regression in the performance evaluation step.

Classification using the selected sets of features was performed with Fisher linear discriminant analysis (FLDA) [31] or using neural networks with radial basis functions (RBFs) [34]. The details of the RBF methodology used are provided in one of our previous publications [21]. With each set of features, the architecture of the RBFs was varied by using 1–40 neurons in a hidden layer and using values of the spread parameter from 1 to 8, in steps of 1. The performance criterion used to select the best RBF network among those evaluated was the area under the ROC curve. The leave-one-out (LOO) procedure was used in training and testing each classifier. ROC curves based on the discriminant values derived from the classifiers were obtained using ROCKIT.

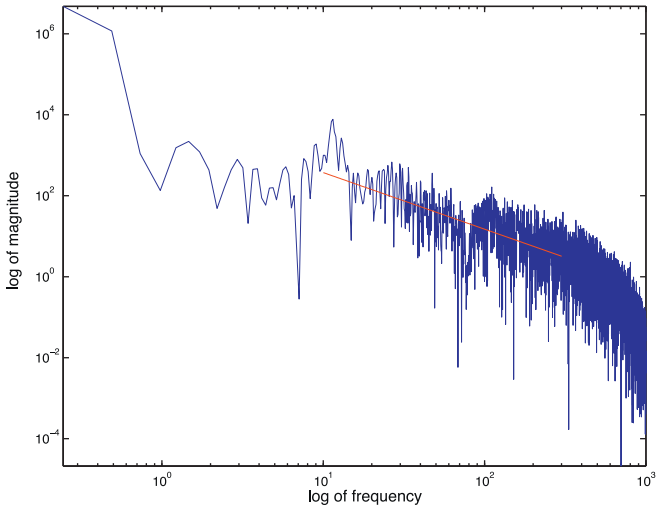

Fig. 4. PSD of the normal VAG signal in Fig. 2 with the straight-line fit to the range [10, 300] Hz. FD = 1.801.

4. Results

4.1. Results with synthesized fBm signals

The estimated FD values for the four synthesized signals shown in Fig. 1 are given in the caption of the figure. The root-mean-squared (RMS) error between the known and estimated values of FD for the 110 synthesized signals was computed to be 0.0198, which indicates accurate estimation of the FD by the PSA method. The PSA method performed well with the synthesized signals for FD in the range of [1.1, 1.8], but overestimated FD values in the range [1.9, 2.0].

Estimates of FD were also obtained for the synthesized fBm signals using the well-known and popular box counting and ruler methods; the two methods led to slightly poorer results, with higher RMS errors of 0.1387 and 0.2243, respectively. The results indicate that the PSA method is the best suited method for the estimation of FD of fBm and self-affine signals, among the three methods studied.

4.2. Results with FD of VAG signals

Figs. 4 and 5 show the PSDs and the linear fits derived to estimate the FD of the normal and abnormal VAG signals shown in Figs. 2 and 3, respectively. The estimated FD values for the two signals are given in the captions of Figs. 4 and 5. The average and standard deviation values of FD for the 51 normal signals were 1.8061 ± 0.2398; those for the 38 abnormal VAG signals were 1.6695 ± 0.2226 (using the frequency range [10, 300] Hz). The discriminant capability of the FD values was assessed in terms of the area (A_z) under the ROC curve by using ROCKIT [29]. The FD values obtained by the PSA method applied to the full VAG signals led to $A_z = 0.6872$.

The values of FD estimated for the first half (extension) and second half (flexion) of each signal led to poorer A_z values of 0.6133 and 0.5916, respectively. With the FD values derived using quarter portions of the VAG signals, the four parts, in order, led to $A_z = 0.6546$, 0.7394, 0.5959, and 0.7023 (using the frequency range [10, 380] Hz). The various A_z values obtained are listed in Table 1 for

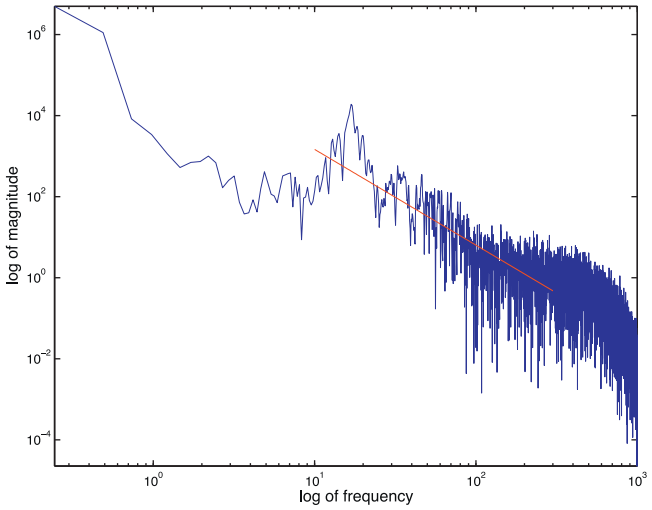

Fig. 5. PSD of the abnormal VAG signal in Fig. 3 with the straight-line fit to the range [10, 300] Hz. FD = 1.319.

Table 1
Area under the ROC curve for various features and combinations thereof (obtained using ROCKIT) and *p*-values indicating the statistical significance of the differences in the individual features between the normal and abnormal categories (obtained via the *t*-test). FD: fractal dimension of the complete duration of a VAG signal. FD1h and FD2h: FD of the first and second halves of a VAG signal. FD1q, FD2q, FD3q, and FD4q: FD of the first, second, third, and fourth quarters of a VAG signal. The two sets of features listed were selected by SFS and SBS; classification was performed using FLDA and the LOO method.

Features	A_z	*p*-Value
FD	0.6872	0.0075
FD1h	0.6133	0.0850
FD2h	0.5916	0.0573
FD1q	0.6546	0.0222
FD2q	0.7394	0.0001
FD3q	0.5959	0.0813
FD4q	0.7023	0.0003
{FD2q, FD4q, FD1q, FD1h, FD2h}	0.7394	–
{FD2q, FD, FD4q, FD1q, FD1h}	0.7510	–

easy comparison. Table 1 also provides the *p*-values indicating the statistical significance of the differences in the features between the normal and abnormal categories (obtained via the *t*-test). It is evident from the *p*-values that the differences between the values of FD, FD2q, and FD4q are statistically highly significant ($p < 0.01$), whereas the differences in the FD1q values for the normal and abnormal categories are statistically significant ($0.01 < p < 0.05$). Thus, the usefulness of some of the FD-based parameters in discriminating between normal and abnormal VAG signals is established.

The seven FD values obtained were analyzed using the SFS and SBS procedures. The SFS procedure selected the set of features {FD2q, FD4q, FD1q, FD1h, FD2h}, in order, whereas the SBS procedure selected the set {FD2q, FD, FD4q, FD1q, FD1h}, in order, which provided $A_z = 0.7394$ and 0.7510, respectively, with the FLDA and LOO procedures. The result provided by the combination of features selected by SBS is only marginally better than that provided by FD2q on its own; however, combinations of features may be expected to provide more robustness and better generalization capabilities than individual features. The best results obtained with RBFs are as follows: with an RBF having 6 nodes in the hidden layer and a spread parameter of 3, the SFS features provided $A_z = 0.7436$; the SBS features provided $A_z = 0.7380$ with an RBF having 5 nodes in the hidden layer and a spread parameter of 1. The lack of improvement in classification performance with the selected combinations of features could be due to correlation being present between the various FD parameters and limitations of the SFS and SBS methods in selecting optimal sets of features.

4.3. Analysis of combination with other features

In our previous studies [21–23] with the same dataset of VAG signals as in the present study, we had derived the following features:

- the form factor (FF) for the full duration of each VAG signal as well as its first half (FF1) and second half (FF2) [21];
- the statistical parameters skewness (S_d), kurtosis (K_d), and entropy (H_d) estimated using the VAG signal samples directly [21];
- the turns count for the full duration (TC), the first half (TC1), and the second half (TC2) of each signal [22];
- the variance of the mean-squared value (VMS) for the full duration, the first half (VMS1), and the second half (VMS2) of each signal [22]; and
- the difference between the Kullback–Leibler distances to the normal and abnormal probability density functions or PDFs (dKLD), mean (μ), standard deviation (σ), coefficient of variation (CV = σ/μ), skewness (S), kurtosis (K), and entropy (H), with VAG signal PDFs estimated using Parzen windows [23].

The best classification performance reported in our previous studies, using RBFs, are as follows: $A_z = 0.82$ with {FF1, FF2, S_d, K_d, H_d } [21]; $A_z = 0.9174$ with {TC1, TC2} [22]; and $A_z = 0.8322$ with {dKLD, K, H, μ, σ} [23].

In the present study, the seven features derived via fractal analysis (see Table 1) were tested further in combination with the features derived in our previous studies, as listed above. The features S_d, K_d, and H_d were not used due to the availability of the same features derived using Parzen PDFs (listed above as S, K, and H). Thus, 23 features were available for each VAG signal. The features were processed with the SFS and SBS procedures. The set of features selected by SFS is {FF1, dKLD, TC1, FD2q, FD1q, S}. The set of features selected by SBS is {FF1, dKLD, TC1, VMS, FD2q, FF, FD4q, TC2, σ, H, S, K, FD1h}. The results indicate that the features derived from all of the methods used in our previous and present studies can contribute in a complementary manner to the classification of VAG signals. The sets of features selected by SFS and SBS, when processed with FLDA and the LOO method, resulted in good classification performance with $A_z = 0.7087$ and 0.7386, respectively; however, due to the increased number of features, these results are slightly worse than those obtained by using combinations of the FD parameters derived in the present study.

Using the set of six features selected by SFS, RBF networks having a single neuron in the hidden layer and a spread parameter of 1, 2, 3, or 4 resulted in $A_z = 0.9610$; a single neuron in the hidden layer and a spread parameter of 6, 7, or 8 resulted in $A_z = 0.9210$; two neurons in the hidden layer and a spread parameter of 1, 2, 3, or 4 resulted in $A_z = 0.9470$; and two neurons in the hidden layer and a spread parameter of 6, 7, or 8 resulted in $A_z = 0.9210$. An exceptional classification result achieved was $A_z = 1.0$ with an RBF using a single neuron in the hidden layer and a spread parameter of 5. The larger set of 13 features selected by SBS provided comparable results (without the case of $A_z = 1.0$).

The results with RBFs indicate that high performance in screening of VAG signals may be obtained by using selected combinations of the features we have proposed in the present and previous works. A small set of six selected features has resulted in nearly perfect classification with relatively simple RBF networks. However, given the small size of the dataset used (89 signals), the possibility exists that the RBF networks are trained to the specific characteristics of the dataset (regardless of the LOO method of cross validation used),

and that the classifiers may not generalize well to other datasets. Notwithstanding these observations, the results obtained in the present study are noteworthy and indicate the high potential of screening for knee-joint abnormalities using VAG signals.

5. Discussion

The FD values for abnormal VAG signals were observed to be, on the average, lower than those for normal signals (see Table 1). This could be interpreted as follows. The presence of defects in the articular surfaces of the knee joint due to loss or shedding of cartilage leads to structured vibration components that disrupt or replace the random, fBm-like signals associated with the normal friction-free cartilage surfaces. Although the VAG signals of some normal knees could possibly contain nonrandom components, such as clicks and crepitus, they would be fewer and occur less often than the grinding noise components found in abnormal knee joints. The disruption of the fBm-like characteristics of normal VAG signals by pathological conditions may be expected to result in lower FD values for abnormal VAG signals via the PSA approach and the $1/f$ model. The range of the FD values of the abnormal VAG signals in the present study agrees with the ranges of FD of acceleration signals obtained from finger joints of patients with calcium pyrophosphate deposition disease, rheumatoid arthritis, or spondyloarthropathy in the study of Shah et al. [10] (see Section 1.2).

The classification performance of the features derived via fractal analysis, with the highest A_z value 0.74 in ROC analysis, is comparable to the performance provided by several features obtained by linear prediction modeling, cepstral analysis, measures of variability of power, turns count, probabilistic models, wavelets, and time-frequency distributions [16,17,20–23]. Selected combinations of FD with some of the other features mentioned above have led to better results with A_z values in the range [0.92, 0.96] and an exceptional case of perfect classification ($A_z = 1.0$) of the 89 VAG signals in the dataset used.

The present work has been limited to classification of normal versus abnormal VAG signals, that is, screening. It would be desirable to extend the classification procedure to various subcategories of knee-joint pathology before the methods become suitable for clinical application.

6. Conclusion

The present work establishes the usefulness of fractal analysis of VAG signals with the PSA method and the $1/f$ model. It would be desirable to test the methods with a larger database and cross validate their performance with multiple independent databases including subcategories of knee-joint pathology. The various methods and features proposed in our works should find use in early detection and monitoring of knee-joint pathology.

Acknowledgments

R.M. Rangayyan has been supported by the University Professorship of the University of Calgary. Y.F. Wu and S.X. Cai have been supported by the Fundamental Research Funds for the Central Universities of China (grant numbers 2010121061 and 2010121062), the Natural Science Foundation of Fujian Province of China (grant no. 2011J01371), the National Natural Science Foundation of China (grant no. 81101115), Xiamen University Undergraduate Fundamental Innovation Research Grant number CXB2011023, and Xiamen University Undergraduate Student Innovative Experiment Project Grant number XDDC2011007.

References

[1] B.B. Mandelbrot, Fractal Geometry of Nature, W.H. Freeman, San Francisco, CA, 1983.
[2] R.F. Voss, Random fractal forgeries, in: R.A. Earnshaw (Ed.), Fundamental Algorithms for Computer Graphics, Springer-Verlag, New York, NY, 1985.
[3] R.F. Voss, Fractals in nature: from characterization to simulation, in: H.O. Peitgen, D. Saupe (Eds.), The Science of Fractal Images., Springer-Verlag, New York, NY, 1988.
[4] A.L. Goldberger, Fractal mechanisms in the electrophysiology of the heart, IEEE Engineering in Medicine and Biology Magazine 11 (1992) 47–52.
[5] A.L. Goldberger, V. Bhargava, B.J. West, A.J. Mandell, On a mechanism of cardiac electrical stability: the fractal hypothesis, Biophysical Journal 48 (1985) 525–528.
[6] S. Abboud, O. Berenfeld, D. Sadeh, Simulation of high-resolution QRS complex using a ventricular model with a fractal conduction system, Circulation Research 68 (1991) 1751–1760.
[7] A.L. Goldberger, B.J. West, Fractals in physiology and medicine, The Yale Journal of Biology and Medicine 60 (1987) 421–435.
[8] X. Li, J. Polygiannakis, P. Kapiris, A. Peratzakis, K. Eftaxias, X. Yao, Fractal spectral analysis of pre-epileptic seizures in terms of criticality, Journal of Neural Engineering 2 (2005) 11–16.
[9] Z. Liang, D. Li, G. Ouyang, Y. Wang, L.J. Voss, J.W. Sleigh, X. Li, Multiscale rescaled range analysis of EEG recordings in sevoflurane anesthesia, Clinical Neurophysiology 123 (2012) 681–688.
[10] E.N. Shah, N.P. Reddy, B.M. Rothschild, Fractal analysis of acceleration signals from patients with CPPD, rheumatoid arthritis, and spondyloarthroparthy of the finger joint, Computer Methods and Programs in Biomedicine 77 (3) (2005) 233–239.
[11] C.J. Stam, Nonlinear dynamical analysis of EEG and MEG: review of an emerging field, Clinical Neurophysiology 116 (2005) 2266–2301.
[12] M.L. Chu, I.A. Gradisar, L.D. Zavodney, Possible clinical application of a noninvasive monitoring technique of cartilage damage in pathological knee joints, Journal of Clinical Engineering 3 (1) (1978) 19–27.
[13] G.F. McCoy, J.D. McCrea, D.E. Beverland, W.G. Kernohan, R.A.B. Mollan, Vibration arthrography as a diagnostic aid in diseases of the knee, The Journal of Bone and Joint Surgery 69-B (2) (1987) 288–293.
[14] K.O. Ladly, C.B. Frank, G.D. Bell, Y.T. Zhang, R.M. Rangayyan, The effect of external loads and cyclic loading on normal patellofemoral joint signals, Special Issue on Biomedical Engineering, Defence Science Journal (India) 43 (July) (1993) 201–210.
[15] N.P. Reddy, B.M. Rothschild, M. Mandal, V. Gupta, S. Suryanarayanan, Noninvasive acceleration measurements to characterize knee arthritis and chondromalacia, Annals of Biomedical Engineering 23 (1995) 78–84.
[16] R.M. Rangayyan, S. Krishnan, G.D. Bell, C.B. Frank, K.O. Ladly, Parametric representation and screening of knee joint vibroarthrographic signals, IEEE Transactions on Biomedical Engineering 44 (November (11)) (1997) 1068–1074.
[17] S. Krishnan, R.M. Rangayyan, G.D. Bell, C.B. Frank, Adaptive time-frequency analysis of knee joint vibroarthrographic signals for noninvasive screening of articular cartilage pathology, IEEE Transactions on Biomedical Engineering 47 (June (6)) (2000) 773–783.
[18] C.-C. Jiang, J.-H. Lee, T.-T. Yuan, Vibration arthrometry in the patients with failed total knee replacement, IEEE Transactions on Biomedical Engineering 47 (February (2)) (2000) 218–227.
[19] N.P. Reddy, B.M. Rothschild, E. Verrall, A. Joshi, Noninvasive measurement of acceleration at the knee joint in patients with rheumatoid arthritis and spondyloarthropathy of the knee, Annals of Biomedical Engineering 29 (12) (2001) 1106–1111.
[20] K. Umapathy, S. Krishnan, Modified local discriminant bases algorithm and its application in analysis of human knee joint vibration signals, IEEE Transactions on Biomedical Engineering 53 (March (3)) (2006) 517–523.
[21] R.M. Rangayyan, Y.F. Wu, Screening of knee-joint vibroarthrographic signals using statistical parameters and radial basis functions, Medical & Biological Engineering & Computing 46 (3) (2008) 223–232.
[22] R.M. Rangayyan, Y.F. Wu, Analysis of vibroarthrographic signals with features related to signal variability and radial basis functions, Annals of Biomedical Engineering 37 (1) (2009) 156–163.
[23] R.M. Rangayyan, Y.F. Wu, Screening of knee-joint vibroarthrographic signals using probability density functions estimated with Parzen windows, Biomedical Signal Processing and Control 5 (1) (2010) 53–58.
[24] Y.F. Wu, S. Krishnan, R.M. Rangayyan, Computer-aided diagnosis of knee-joint disorders via vibroarthrographic signal analysis: a review, Critical Reviews in Biomedical Engineering 38 (2) (2010) 201–224.
[25] R.M. Rangayyan, F. Oloumi, Fractal analysis of knee-joint vibroarthrographic signals., in: Proc. 10th IEEE International Conference on Information Technology and Applications in Biomedicine (ITAB 2010), IEEE, Corfu, Greece, November, pp. 1–4, 2010.
[26] D. Saupe, Algorithms for random fractals, in: H.O. Peitgen, D. Saupe (Eds.), The Science of Fractal Images., Springer, New York, NY, 1988.
[27] C.E. Metz, ROC methodology in radiologic imaging, Investigative Radiology 21 (1986) 720–733.
[28] C.E. Metz, Basic principles of ROC analysis, Seminars in Nuclear Medicine VIII (4) (1978) 283–298.

[29] ROCKIT. Kurt Rossmann Laboratories for Radiologic Image Research. ROC Software. http://www-radiology.uchicago.edu/krl/roc_soft6.htm, website last accessed April 2010.
[30] J.H. Ware, F. Mosteller, F. Delgado, C. Donnelly, J.A. Ingelfinger, *P* values, in: J.C. Bailar III, F. Mosteller (Eds.), Medical Uses of Statistics, 2nd edition, NEJM Books, Boston, MA, 1992, pp. 181–200.
[31] R.O. Duda, P.E. Hart, D.G. Stork, Pattern Classification, 2nd edition, Wiley, New York, NY, 2001.
[32] B. Sahiner, H.P. Chan, N. Petrick, R.F. Wagner, L. Hadjiiski, Feature selection and classifier performance in computer-aided diagnosis: the effect of finite sample size, Medical Physics 27 (7) (2000) 1509–1522.
[33] R.J. Nandi, A.K. Nandi, R.M. Rangayyan, D. Scutt, Classification of breast masses in mammograms using genetic programming and feature selection, Medical & Biological Engineering & Computing 44 (2006) 683–694.
[34] S. Haykin, Neural Networks: A Comprehensive Foundation, 2nd edition, Prentice Hall, Upper Saddle River, NJ, 1999.